Korean J. Chem. Eng., **25**(6), 1239-1244 (2008)

Onset of buoyancy-driven convection in melting from below

Min Chan Kim*,†, Dong Won Lee, and Chang Kyun Choi*****

*Department of Chemical Engineering, Cheju National University, Cheju 690-756 Korea
**Department of Mechanical Engineering, Cheju National University, Cheju 690-756 Korea
***School of Chemical and Biological Engineering, Seoul National University, Seoul 151-744 Korea
(*Received 29 August 2007 • accepted 1 April 2008*)

Abstract−When a horizontal homogeneous solid is melted from below, convection can be induced in a thermally unstable melt layer. In this study the onset of buoyancy-driven convection during time-dependent melting is investigated by using similarly transformed disturbance equations. The critical Rayleigh numbers based on the melt-layer thickness are found numerically for various conditions. For small superheats, the present predictions approach the well known results of classical Rayleigh-Bénard problems, that is, critical Rayleigh numbers are located between 1,296 and 1,708, regardless of the Prandtl number. However, for high superheats the critical Rayleigh number increases with an increase in phase change rate but with decrease in Prandtl number.

Key words: Buoyancy Driven Convection, Melting, Stefan Problem, Similar Transform

INTRODUCTION

The onset of convective instability in a horizontal fluid layer has been studied extensively since Bénard's and Rayleigh's famous work. Recently, the hydrodynamic stability associated with melting or solidification has attracted many researchers' interests [1-4]. However, due to the intrinsic complexities associated with phase change processes, hydrodynamic stability during melting has not been studied as much. Convective motion near the phase changing interface affects the local temperature and concentration fields which control the geometric characteristics of the interface and melting or solidification rate. So, the convective motion driven by buoyancy forces in melting processes plays an important role in industrial applications, such as metallurgical processes, latent heat thermal energy storage, oceanography, food processing and nuclear reactor safety (see Goldstein and Ramsey [5], Ostrach [6] and Feldman et al. [7]). Thus, a fundamental understanding of convective stability in such a range of applications is very important.

Previous studies [1,8] examined the coupled effects on stability arising from thermal convection and melting/solidification under assumptions where solid/liquid interface position is an invariant with respect to time or it moves at a fixed velocity. In these studies, the solid phase is excluded in their analysis and the effect of the Prandtl number on the onset condition is ignored under the static assumption, despite a melting process usually occurring for various Prandtl numbers. The solid/liquid interface position moves with constant velocity; however, the solid/liquid interface position is determined by an energy balance near the phase- changing interface.

In this study, the time-dependent melting of solid heated from below, the so-called Stefan problem, is considered. When the temperature profiles in the solid and melt phase and also the liquid layer thickness vary with time, the onset conditions of buoyancy-driven convection are analyzed theoretically under the Boussinesq approximation. The time-dependent linearized disturbance equations are transformed similarly and self-similar disturbance equations are solved numerically.

GOVERNING EQUATIONS

The system considered here consists of a semi-infinite solid layer heated from below, as shown in Fig. 1. For time $t \geq 1$, the bottom boundary of the solid is superheated at a constant temperature T_A and the melted layer grows from below. The coordinate system is fixed at the bottom boundary, and the position of the solid/liquid interface is moving in the *Z*-direction. For this system, the variations of the physical properties such as density, viscosity and thermal conductivity are at most 1 per cent for variations in temperature not exceeding 10 K. Therefore, under the Boussinesq approximation, the variations of this small amount can be generally ignored, except for the density variation which is the driving force of the

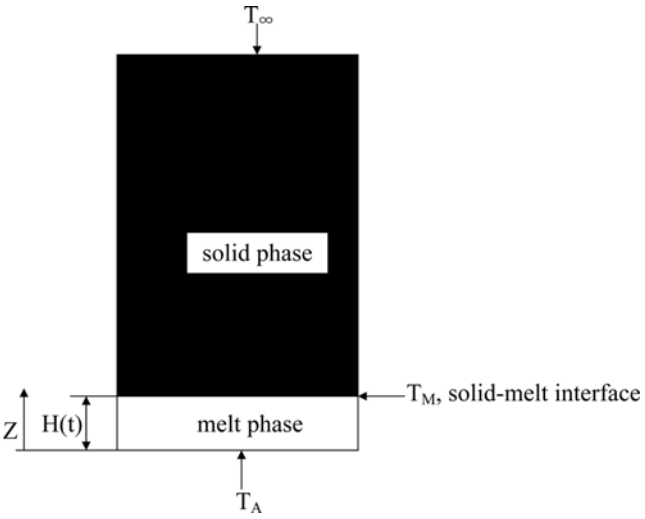

Fig. 1. Schematic diagram of system considered here.

†To whom correspondence should be addressed.
E-mail: mckim@cheju.ac.kr

buoyancy-driven convection [9]. Under this simplification, the governing equations in the melt layer are given by

$$\nabla \cdot \mathbf{U} = 0, \tag{1}$$

$$\left\{\frac{\partial}{\partial t} + \mathbf{U}\cdot\nabla\right\}\mathbf{U} = -\nabla P + \mu\nabla^2\mathbf{U} + \rho_L\mathbf{g}, \tag{2}$$

$$\frac{\partial T_L}{\partial t} + \mathbf{U}\cdot\nabla T_L = \alpha_L\nabla^2 T_L, \tag{3}$$

$$\rho_L = \rho_r[1-\beta(T_L - T_r)], \tag{4}$$

where $\mathbf{U}$ denotes the velocity vector, μ the viscosity, P the pressure, ρ the density, β the thermal expansion coefficient, T the temperature, $\mathbf{g}$ the gravitational acceleration vector, t the time, and α the thermal diffusivity. The subscripts L and r represent the liquid phase and the reference state, respectively. For the present system, the initial state is motionless and therefore, the basic velocity and pressure fields are $\mathbf{U}_0=\mathbf{0}$ and $\nabla P_0=\rho_L\mathbf{g}$, respectively.

For the solid layer the temperature field can be described by

$$\frac{\partial T_S}{\partial t} = \alpha_S\nabla^2 T_S. \tag{5}$$

The subscript S represents the solid phase and the densities of solid and melt are assumed to be equal, i.e., a volume change during the melting process is neglected. The boundary conditions are given as follows:

$$W=0,\ T_L=T_A \text{ at } Z=0, \tag{6a,b}$$

$$W=0,\ \ T_S=T_L=T_M,\ \ k_S\frac{dT_S}{dZ} - k_L\frac{dT_L}{dZ} = \Delta H_f\frac{dH}{dt}$$

$$\text{at } \ Z=H(t)=2\lambda\sqrt{\alpha_L t}, \tag{6c,d,e}$$

$$W=0,\ T_S=T_\infty \text{ at } Z=\infty, \tag{6f,g}$$

where ΔH_f is the latent heat of melting and $H(t)(=\lambda\sqrt{4\alpha_L t})$ the location of melt-solid interface, T_M the melting temperature at the solid-melt interface and T_∞ the temperature of solid far from the interface.

The basic thermal conduction equations are nondimensionalized as

$$\frac{\partial\theta_{0,S}}{\partial\tau} = \alpha_R\nabla^2\theta_{0,S}, \tag{7}$$

$$\frac{\partial\theta_{0,L}}{\partial\tau} = \nabla^2\theta_{0,L}, \tag{8}$$

under the following boundary conditions,

$$\theta_{0,L}=0 \text{ at } \zeta=0, \tag{9a}$$

$$\theta_{0,S}=\theta_{0,L}=-1,\ \ k_r\frac{d\theta_{0,S}}{dz} - \frac{d\theta_{0,L}}{dz} = St\frac{dh}{d\tau} \ \text{ at } \ \zeta=\lambda, \tag{9b,c}$$

$$\theta_{0,S}=-\theta_\infty \text{ at } \zeta=\infty \tag{9d}$$

where $\theta_{0,S}=(T_S-T_A)/(T_A-T_M)$, $\theta_{0,L}=(T_L-T_A)/(T_A-T_M)$, $\alpha_r=\alpha_S/\alpha_L$, $k_r=k_S/k_L$, $z=Z/d$, $h=H/d$, the Stefan number $St=\Delta H_f/[c(T_A-T_M)]$ and d an arbitrary length scale. The solution subjected to the above equations and boundary conditions are given in Carslaw and Jaeger's book [9];

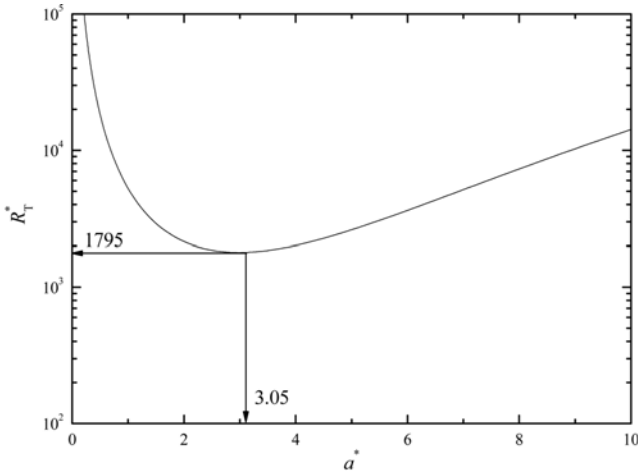

Fig. 2. Marginal stability curve for Pr=1, λ=1, α_r=1 and k_r=1.

$$\theta_{0,S} = -\theta_\infty + (\theta_\infty - 1)\frac{\mathrm{erfc}(\zeta/\sqrt{\alpha_r})}{\mathrm{erfc}(\lambda/\sqrt{\alpha_r})} \ \text{ for } \zeta>\lambda, \tag{10}$$

$$\theta_{0,L} = -\frac{\mathrm{erfc}(\zeta)}{\mathrm{erfc}(\lambda)} \ \text{ for } \zeta<\lambda, \tag{11}$$

where $\zeta=z/\sqrt{4\tau}$. The base temperature for the specific case is shown in Fig. 2. The phase change rate λ can be determined by using Eqs. (9c), (10) and (11) as

$$\frac{\exp(-\lambda^2)}{\mathrm{erf}(\lambda)} - \frac{k_r}{\sqrt{\alpha_r}}(\theta_\infty - 1)\frac{\exp(\lambda^2/\alpha_r)}{\mathrm{erfc}(\lambda/\sqrt{\alpha_r})} = \lambda\sqrt{\pi}St. \tag{12}$$

For the limiting case of θ_∞=1, i.e. $T_\infty=T_M$, the phase change rate λ can be determined from the solution of $1/\lambda(\exp(-\lambda^2)/\mathrm{erf}(\lambda))=T\sqrt{\pi}St$. This equation is independent of α_r and k_r, and it can be further simplified to $\lambda^2\sim1/(2St)$ for a large St. It seems that the above solution is more reasonable than Smith's [8] and Hwang's [10]. They assumed that the planar interface is moving with a constant velocity V_0, and therefore the solid-melt interface position is given by $H(t)=V_0t$. Boger and Westwater [11] measured the interfacial velocities for the melting and freezing process of a water-ice system. Their experimental results show that a constant-velocity model is not physically realistic.

Under linear stability theory the physical variables are decomposed into the unperturbed quantities and their perturbed ones at the onset of convection. In the melt layer the dimensionless disturbance equations are obtained as

$$\frac{\partial\theta_{1,L}}{\partial\tau} + R_T W_1\frac{\partial\theta_{0,L}}{\partial z} = \nabla^2\theta_{1,L}, \tag{13}$$

$$\left(\frac{1}{Pr}\frac{\partial}{\partial\tau} - \nabla^2\right)\nabla^2 W_1 = -\nabla_1^2\theta_{1,L}, \tag{14}$$

where the subscript 1 denotes the perturbed quantities, W the vertical velocity component, and $R_T=(g\beta\Delta Td^3/\alpha_L\nu)$ the Rayleigh number. Note that θ_1 has the scale of $\alpha_L\nu/(g\beta d^3)$ and w_1 has the scale of α_L/d. Here ν is the kinematic viscosity of melt phase. Eq. (14) is obtained by taking the double curls on Eq. (2). Through this procedure, the pressure term is eliminated. The whole procedure to derive Eqs. (13) and (14) is well described in Chandrasekhar's book [9].

In the solid layer the dimensionless disturbance equations are obtained as

$$\frac{\partial \theta_{1,S}}{\partial \tau} = \alpha_r \nabla^2 \theta_{1,S}. \quad (15)$$

The boundary conditions for these disturbance equations are given by

$$\theta_{1,S}=0 \text{ at } z=\infty, \quad (16a)$$

$$w_1 = \frac{\partial w_1}{\partial z} = 0, \quad \theta_{1,S} = \theta_{1,L}, \quad k_S D\theta_{1,S} = k_L D\theta_{1,L} \text{ at } z=h, \quad (16b,c\&d)$$

$$w_1 = \frac{\partial w_1}{\partial z} = \theta_{1,L} = 0 \text{ at } z=0. \quad (16d)$$

In the present study the scaling of $W_1 \sim g\beta\Gamma_1 H^2/\nu$ in dimensional form is obtained from Eq. (2). This relation means that $w_1/\theta_1 \sim h^2 \sim \tau$. If disturbance amplitudes follow the property of the base temperature fields shown in the relations (10) and (11), it is probable that $\partial\theta_1/\partial\tau = -(\zeta/(2\tau))(d\theta^*/d\zeta)$, where the superscript "*" represents the similary transformed quantities. Therefore, under the normal mode analysis where an arbitrary disturbance having two-dimensional periodicity is considered [9], the dimensionless amplitude functions of disturbances are assumed to have the relation of

$$[w_1, \theta_{1,L}, \theta_{1,S}] = [\tau w^*(\zeta), \theta_L^*(\zeta), \theta_S^*(\zeta)]\exp[i(a_x x + a_y y)] \quad (17)$$

where a_x and a_y are the horizontal wavenumbers representing two-dimensional periodicity in the x and the y direction, respectively. The above equation means that the amplitude of dimensionless disturbances is assumed to be a function of the similarity variable ζ ($=z/\delta$) where $\delta = \sqrt{4\tau}$. This kind of similarity transformation has been widely used in similar problems [1,4,12,13].

Substituting Eq. (17) into (13)-(15) with $a^2 = a_x^2 + a_y^2$, $\partial/\partial\tau = -(2\zeta/\tau)D$ and $\partial^2/\partial z^2 = (1/4\tau)D^2$ gives the following self-similar stability equations:

$$\left(D^2 + \frac{2}{\alpha_r}\zeta D - a^{*2}\right)\theta_S^* = 0, \quad (18)$$

$$(D^2 + 2\zeta D - a^{*2})\theta_L^* = R_T^* w^* D\theta_{0,L}, \quad (19)$$

$$\left[(D^2 - a^{*2})^2 + \frac{2}{\mathrm{Pr}}(\zeta D^3 - a^{*2}\zeta D + 2a^{*2})\right] w^* = -a^* \theta_L^*, \quad (20)$$

where $D=d/d\zeta$, $R_T^* = R_T\delta^3$, $a^* = a\delta$ and $\delta = \sqrt{4\tau}$. R_T^* and a^* are assumed to be the eigenvalues having the meaning of the Rayleigh number and the wavenumber based on the melt thickness, $H(t)(\propto\sqrt{t})$. The boundary conditions can be reduced as

$$\theta_S^* = 0 \text{ at } \zeta=\infty, \quad (21a)$$

$$w^* = Dw^* = 0, \ \theta_S^* = \theta_L^*, \ k_S D\theta_S^* = k_L D\theta_L^* \text{ at } \zeta=\lambda, \quad (21b,c,d)$$

$$w^* = Dw^* = \theta_L^* = 0 \text{ at } \zeta=0. \quad (21e)$$

The similarity assumption (17) yields the terms $(2/\alpha_r)\zeta D\theta_S^*$, $2\zeta D\theta_L^*$ $1/\mathrm{Pr}(\zeta D^3 - a^{*2}\zeta D + 2a^{*2})$ in Eqs. (18), (19) and (20), respectively. These terms have been neglected in the conventional quasi-static analysis, where the terms of $\partial(\cdot)/\partial\tau$ are assumed to be zero and the stability criteria are obtained independently of the Prandtl number.

SOLUTION METHOD

The stability equation for the solid layer can be solved independently of the melt layer by using the boundary condition (21). By using the WKB approximation [14] the temperature disturbance in the solid layer is approximated as

$$\theta_S^* \sim \frac{C}{\left(\frac{\zeta^2}{\alpha_r^2} + \frac{1}{\alpha_r} + a^{*2}\right)^{1/4}} \exp\left[-\int_\lambda^\zeta \left(\frac{\zeta^2}{\alpha_r^2} + \frac{1}{\alpha_r} + a^{*2}\right)^{1/2} d\zeta\right] \exp\left(-\frac{\zeta^2}{2\alpha_r}\right), \quad (22)$$

which satisfies the upper boundary condition of Eq. (21a). Here C is a constant. By substituting Eq. (22) into the boundary conditions (21c) and (21d), the following condition can be obtained.

$$D\theta_L^* = -k_r\left[\left(\frac{\lambda^2}{\alpha_r^2} + \frac{1}{\alpha_r^2} + a^{*2}\right)^{1/2} + \frac{\lambda}{\alpha_r} + \frac{1}{2}\frac{\lambda}{\alpha_r^2}\left(\frac{\lambda^2}{\alpha_r^2} + \frac{1}{\alpha_r^2} + a^{*2}\right)^{-1}\right]\theta_L^*$$

$$\text{at } \zeta=\lambda. \quad (23)$$

Now, the stability Eq. (19) and (20) should be solved under the boundary conditions (21b), (21c), (21e) and (23). For the limiting case of $k_r=0$ and $k_r=\infty$ the boundary conditions (21c,d) reduce to $D\theta_L^*(\lambda)=0$ and $\theta_L^*(\lambda)=0$.

These stability equations are solved by employing the outward shooting scheme. For a given a^*, λ, k_r and α_r, in order to integrate the above stability equations, the proper values of D^2w^*, D^3w^* and $D\theta^*$ at $\zeta=0$ are assumed. Since the stability equations and their boundary conditions are all homogeneous, the value of $D^2w^*(0)$ can be assigned arbitrarily, and the value of the parameter R_T^* is assumed. This procedure can be understood easily by taking account of the characteristics of eigenvalue problems. After all the values at $\zeta=0$ are provided, this eigenvalue problem can proceed numerically.

Integration is performed from $\zeta=0$ to a melt-solid interface $\zeta=\lambda$ with the fourth order Runge-Kutta-Gill method. If the guessed values of R_T^*, $D^3w^*(0)$ and $D\theta^*(0)$ are correct, the bounday conditions for w^* and θ^* will be satisfied at the melt-solid interface. To improve the initial guesses the Newton-Raphson iteration is used. The marginal stability curve for the typical case is given in Fig. 2. The region above the curve denotes the unstable state, whereas below the curve the system is stable. In the figure the minimum value of R_T^* is the

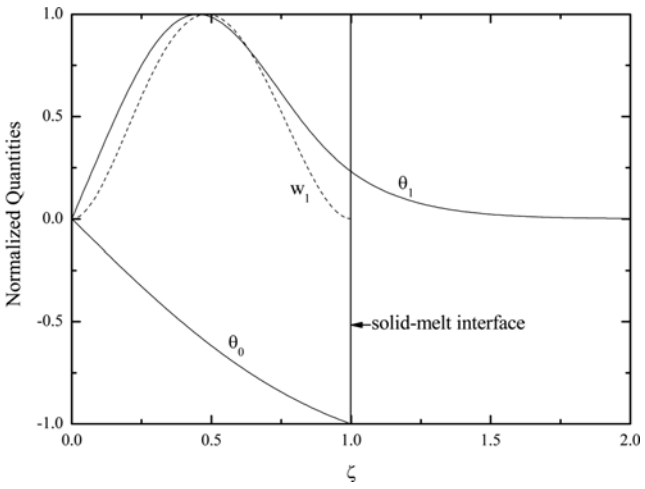

Fig. 3. Normalized distribution of disturbances at critical conditions for Pr=1, λ=1, α_r=1 and k_r=1 with the base temperature distribution for θ_∞=1.

critical condition marking the onset of buoyancy-driven convection. At this condition the disturbance profiles are featured in Fig. 3 with the base temperature profile for θ_∞=1.

RESULTS AND DISCUSSION

The dimensionless parameters governing the present system are St, θ_∞, α_r and k_r. The effects of these parameters on convective instabilities during the melting can be represented by λ through Eq. (12) and the boundary condition (23). For the limiting case of θ_∞=1, the phase change rate λ can be obtained from $1/\lambda\,(\exp(-\lambda^2))/(\mathrm{erf}(\lambda)) = \sqrt{\pi}\,\mathrm{St}$ and therefore, the effects of α_r and k_r on the critical conditions are seen from the boundary condition (23). For a given λ, the stability conditions of the limiting cases of $k_r=\infty$ and k_r=0 are independent of α_r. The stability conditions for these limiting cases are illustrated in Figs. 3 and 4, where $Ra=R_T^*\lambda^3$ and $a=a^*\lambda$ are the Rayleigh number and wavenumber based on the melt thickness H(t). As shown in these figures, for the limiting case of $\lambda\to 0$, the critical Rayleigh number and wavenumber approach the well-known values of Ra_c=1,708 and a_c=3.117 for a conducting boundary, and Ra_c=1,296 and a_c=2.55 for an insulating boundary. These are the critical conditions of classical Rayleigh-Bénard problems [15].

For the limiting case of θ_∞=1, Sparrow et al. [1] conducted stability analysis on the present system by neglecting the temporal growth of disturbances and using the boundary condition of $\theta_L^*(\lambda)$=0. Their quasi-static analysis results show that there exists a minimum Rayleigh number for small-λ cases. However, the minimum one is not observed in the present study. Since Sparrow et al. [14] excluded the solid layer from their analysis, their boundary condition of $\theta_L(\lambda)$= 0 corresponds to that of the limiting case of $k_r=\infty$. As shown in Fig. 4, for small λ the critical Rayleigh numbers are located between 1,296 and 1,708 depending on α_r and the quasi-static assumption is valid. At these limiting cases the distribution of disturbance quantities are featured in Fig. 5. As shown in this figure, the temperature disturbance for $k_r=\infty$ is limited within the melt layer and the system of $k_r=\infty$ is more stable than that of k_r=0. The distributions of disturbance quantities for various Pr cases are featured in Fig. 6. It is known that the vertical position showing w_{max}, i.e. $\zeta|_{w_{max}}$ moves toward the heated surface with decreasing Pr. The vertical position

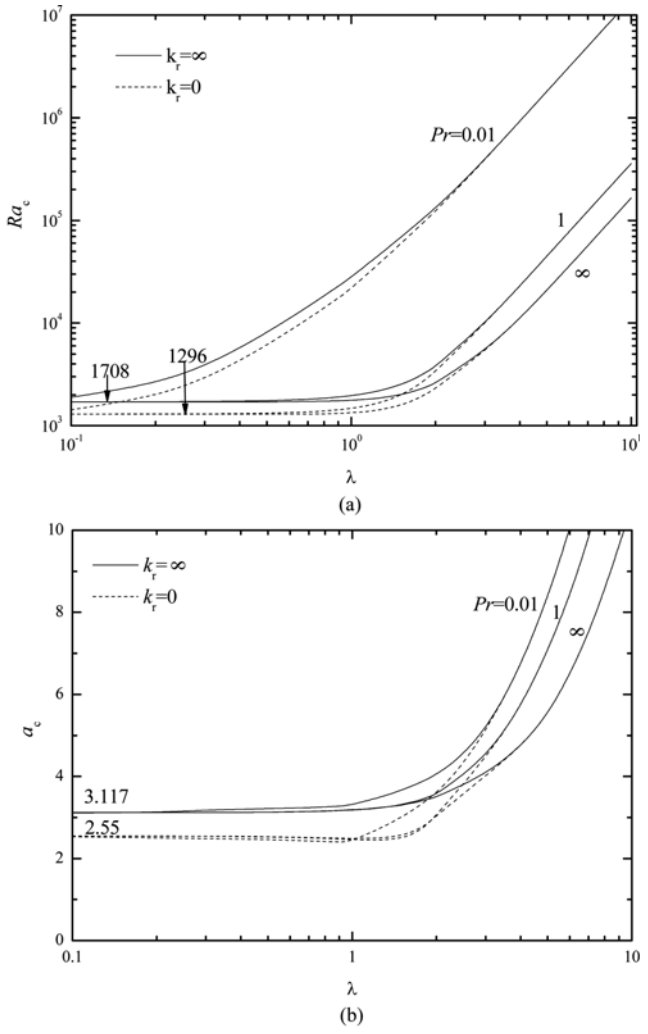

Fig. 4. Critical conditions for limiting cases of $k_r=\infty$ and k_r=0. (a) critical Rayleigh number and (b) critical wavenumber

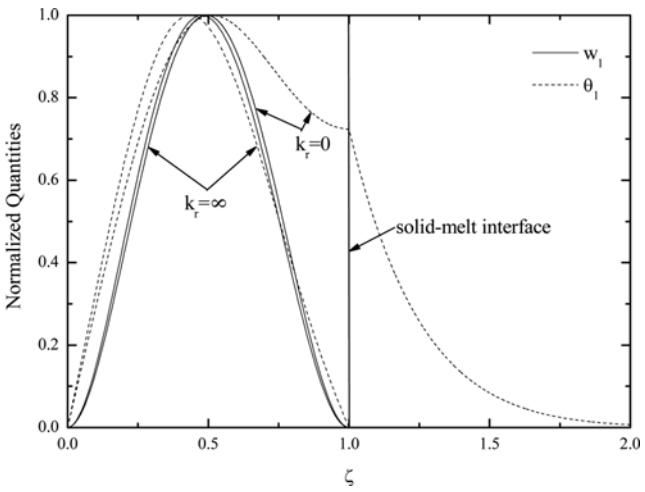

Fig. 5. Normalized distribution of disturbances at critical conditions for Pr=1, λ=1, α_r=1 and the limiting case of $k_r=\infty$ and k_r=0.

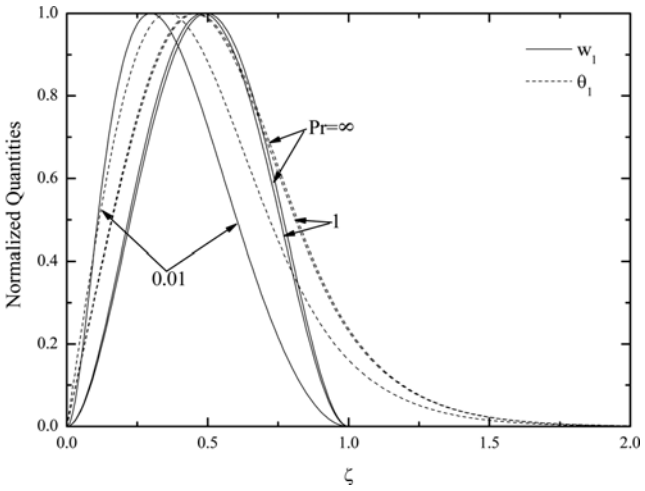

Fig. 6. Normalized distribution of disturbances at critical conditions with λ=1, α_r=1, k_r=1 for various Pr.

showing θ_{max}, i.e., $\zeta|_{\theta_{max}}$ is larger than $\zeta|_{w_{max}}$ for Pr≥1; however, this trend seems to be reversed for Pr<<1.

For λ>3, the basic temperature profile becomes $\theta_{0,L}$=−erf(ζ) and

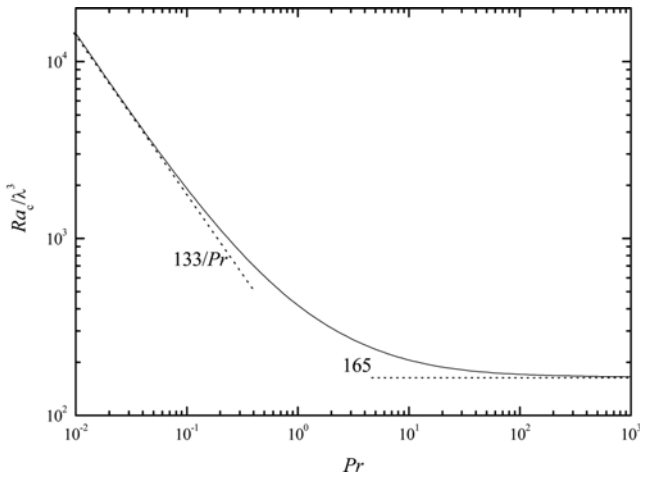

Fig. 7. The effect of Pr on the critical Rayleigh number for a large λ case.

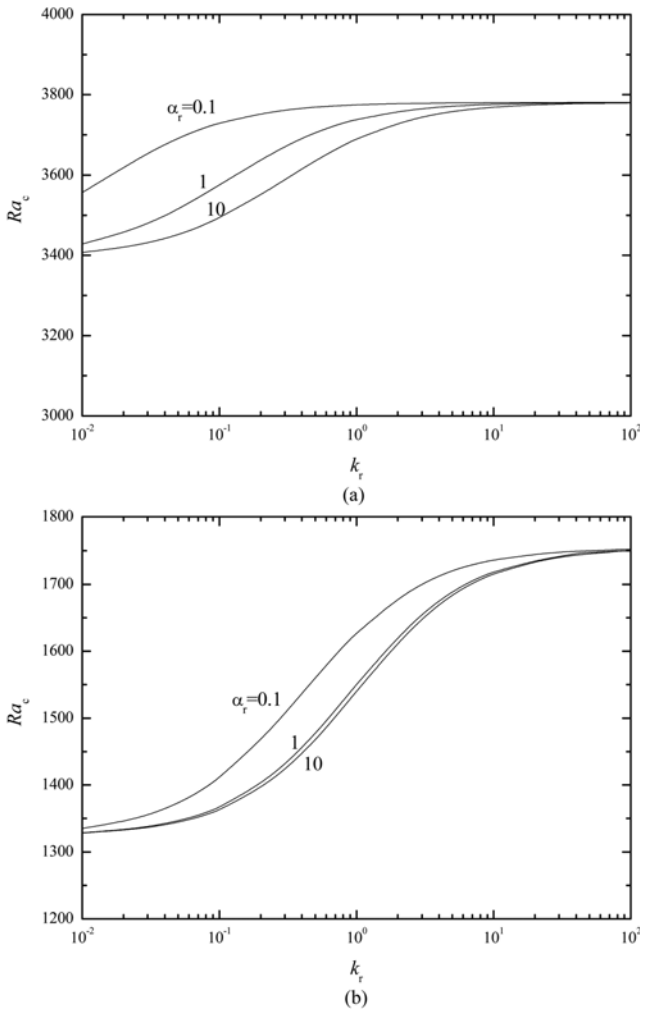

Fig. 8. The effects of k_r and α_r on the critical conditions for Pr=1: (a) λ=2 and (b) λ=0.5.

the effect of boundary conditions on the melt-solid interface on critical conditions is small. For large λ the asymptotic critical conditions are given in Fig. 7. Based on these results, the critical condition to mark the onset of convective motion is correlated as

$$Ra_c = 165\left[1+\left(\frac{0.804}{Pr}\right)^{3/4}\right]^{8/9}\lambda^3 \quad \text{for } \lambda>3, \tag{24}$$

within the error bound of 5%. This condition is independent of the upper boundary conditions. The above correlation shows that Ra_c increases with an increase in λ but with a decrease in Pr. Kim et al. [16] analyzed the onset of buoyancy-driven convection in a horizontal fluid layer heated isothermally from below. Their stability equations which consider the temporal growth of disturbance quantities are identical with the present ones and their stability criteria are almost the same as the present ones. It seems that the onset time of buoyancy-driven convection is independent of the melt thickness H(t) for λ>3.

The effect of k_r on the critical conditions is summarized in Fig. 8 for various α_r with λ=2 and λ=0.5. The critical conditions approach the asymptotic values for k_r=∞ and k_r=0. For the large-α_r case the boundary condition (23) reduces to $D\theta_L^*(\lambda)=-k_r a^* \theta_L^*(\lambda)$ while for the small α_r case, it leads to $D\theta_L^*(\lambda)=-k_r(1+\sqrt{1+\lambda^2})/\alpha_r\theta_L^*(\lambda)$. From this, it can be assumed that the effect of α_r on the critical condition is not significant for large k_r, as shown in Fig. 6. With increasing k_r and α_r, the critical Rayleigh number Ra_c increases and the system becomes more stable.

To validate the theoretical analysis the predictions of τ_c and a_c should be compared with experimental observations. Unfortunately no experimental value is available now. Therefore, the systematic experiments are necessary and opened.

CONCLUSIONS

The onset of buoyancy-driven convection in a homogeneous melt heated from below is analyzed by considering both the melt and the solid phase. The thermal disturbance distribution is approximated by the WKB method and the stability equations in the melt phase are solved numerically. For a slowly heated system, the critical conditions approach the well-known results of classical Rayleigh-Bénard problems, that is, critical Rayleigh numbers are located between 1,296 and 1,708. However, for a rapidly heated system the critical Rayleigh number becomes independent of conditions at the melt-solid interface and highly deviates from the above values.

ACKNOWLEDGMENT

This work was supported by the Korea Energy Management Corporation and Ministry of Commerce, Industry and Energy of Korea as a part of the project of "Constitution of Energy Network using District Heating Energy" in "Energy Conservation Technology R&D" project.

NOMENCLATURE

a : dimensionless wavenumber, $\sqrt{a_x^2+a_y^2}$
a* : dimensionless wavenumber based on the melt thickness, $a\delta$
c : specific heat [J/(kg·K)]

d : arbitrary length scale [m]
g : gravitational acceleration vector [m/s^2]
H : thickness of a melt layer [m]
h : dimensionless thickness of a melt layer, H/d
K : permeability [m^2]
k : thermal conductivity [W/mK]
k_r : thermal conductivity ratio, k_S/k_L
P : pressure [Pa]
R_T : Rayleigh number based on length scale, $g\beta\Delta Td^3/\alpha_L\nu$
R_T^* : Rayleigh number based on melt thickness scale, $R_T\delta^3$
Ra : Rayleigh number based on melt thickness, $g\beta\Delta TH^3/\alpha_L\nu$
St : Stefan number, $\Delta H_f/[c(T_A-T_M)]$
T : temperature [K]
t : time [s]
U : velocity vector [m/s]
w_1 : dimensionless vertical velocity component, W_1d/α_L
(x, y, z) : dimensionless Cartesian coordinates

Greek Letters

α : thermal diffusivity [m^2/s]
α_r : thermal diffusivity ratio, α_S/α_L
β : thermal expansion coefficient [K^{-1}]
ΔH_f : latent heat of melting [J/kg]
δ : dimensionless depth, $\sqrt{4\tau}$
θ_0 : dimensionless basic temperature, $(T-T_A)/(T_A-T_M)$
θ_1 : dimensionless temperature disturbance, $g\beta d^3T_1/(\alpha_L\nu)$
λ : phase change rate
μ : viscosity [Pa·s]
ρ : density [kg/m^3]
τ : dimensionless time, $\alpha_L t/d^2$
ζ : similarity variable, z/δ

Subscripts

c : critical state
L : liquid phase
S : solid phase
0 : basic quantity
1 : perturbed quantity

Superscript

* : similary-transformed quantitiy

REFERENCES

1. E. M. Sparrow, L. Lee and N. Shamsundar, *J. Heat Transfer*, **98**, 88 (1976).
2. C. Gau and R. Viskanta, *Int. J. Heat Mass Transfer*, **28**, 573 (1985).
3. C. F. Chen and F. Chen, *J. Fluid Mech*., **227**, 567 (1991).
4. I. G. Hwang and C. K. Choi, *J. Crystal Growth*, **267**, 714 (2004).
5. R. J. Goldstein and J. W. Ramsey, in *Studies in heat transfer*, A. Festschrift, E. R. G. Eckert, J. P. Hartnet Eds., McGraw-Hill, Washington DC, pp. 199-208 (1978).
6. S. Ostrach, *Trans. ASME: J. Fluids Eng.*, **105**, 5 (1983).
7. D. Feldman, M. M. Shapiro, D. Banu and C. J. Fuks, *Solar Energy Mater.*, **18**, 201 (1989).
8. M. K. Smith, *J.Fluid Mech*., **188**, 547 (1988).
9. H. S. Carslaw and J. C. Jaeger, *Conduction of heat in solids*, 2nd ed., Oxford Univ. Press (1959).
10. I. G. Hwang, *AIChE J*., **47**, 1698 (2001).
11. D. V. Boger and J. W. Westwater, *Trans. ASME: J. Heat Transfer*, **89**, 81 (1967).
12. R. P. Lowell, *J. Volcanol. Geotherm. Res*., **26**, 1 (1985).
13. M. C. Kim, T. J. Chung and C. K. Choi, *Kor. J. Chem. Eng*., **21**, 69 (2004).
14. J. Mathews and R. L. Walker, *Mathematical methods of physics*, 2nd ed., W.A. Benjamin Inc. (1970).
15. E. M. Sparrow, R. J. Goldsetin and V. K. Jonsson, *J. Fluid Mech.*, **18**, 513 (1964).
16. M. C. Kim, H. K. Park and C. K. Choi, *Theoret. Comput. Fluid Mech*., **16**, 49 (2002).